Chapter 3

Structures of Intercalated Ions in Saponite and Tetrasilicicfluormica

3.1 X-Ray Powder Diffraction (XRD)

X-ray powder diffraction patterns observed at 300±1 and 400±2 K in Na-SP and Na-MC are shown in Fig. 3.1 and 3.2, respectively. Fig. 3.3-15 show results in XRD measurements for all intercalation compounds employed in this study. *d*(001) spacings and interlayer distances in Na-SP, Na-MC and the other intercalation compounds were obtained by subtraction of the layer thickness, 9.6 Å [7], from the observed basal spacings obtained from (001) reflections, and are listed in Table 3.1 and 3.2. From the diffraction patterns in Fig. 3.1, the interlayer distance in Na-SP was shown to be decreased with rising temperature. This result is attributable to the desorption of water molecules hydrated to Na^+ ions in the interlayer space, because the desorption of hydration molecules was already confirmed to take place at *ca.* 350 K in the TG-DTA measurement by Kunimine Industries. Therefore, the interlayer spacing of Na-SP with no interlayer water except tightly hydrated one around Na^+ ions, is ca. 0.6 Å estimated from the value observed at 400 K. As for Na-MC, the interlayer spacing is nearly 0 Å, indicating that the small and spherical Na^+ ions fall in openings made by six surrounding oxygen atoms on the clay wall as shown in Fig. 3.17 and no room exists

between clay sheets before the intercalation of organic cations. The interlayer spacings obtained for all intercalated samples determined at both 300 and 400 K were larger than those in Na-SP and Na-MC. This fact means organocations bigger than Na^+ ions, are intercalated between clay sheets. The interlayer spacings in the range of 3.2-4.1 Å were obtained for specimens containing straight-chain alkylammonium ions. Since these values are close to the short diameter (ca. 4.2 Å) of the cross section perpendicular to the molecular long-axis estimated from alkyl chains with the trans-zigzag conformation, it can be seen that intercalated alkylammonium ions are arranged with their long axes parallel to the clay sheets. In Gu-SP, and Gu-MC, interlayer spacings of 2.4, and 2.5 Å, respectively, were obtained. These values are shorter than the thickness of guanidinium ion by 1 Å. This fact means that plate-like guanidinium ions are flatly placed on the clay sheet and they get in the clay openings from consideration of the small size of cation. Since the interlayer distance of 2.8 Å evaluated in M3-MC accords with a difference obtained by subtracting the N-H distance, 1.1 Å, and van der Waals radius of H atom, 1.2 Å from the molecular thickness of trimethylammonium ion, 5 Å, it is provable that a trimethylammonium ion exists with a hydrogen atom of its N-H part completely inside the clay opening. As regards M4-MC, a interlayer distance of 3.7 Å was obtained. This value is shorter than 5.4 Å of the minimum length of a tetramethylammonium ion by 1.7 Å and 6.4 Å of the maximum value by 2.7 Å. Although it is difficult to determine the cationic orientation in the interlayer space due to the nearly spherical symmetry in its shape, hydrogen atoms of methyl groups can be embedded in the opening of the sheet to some extent. It is also predicted from the small temperature dependence of interlayer

distances in almost all intercalation compounds that large-amplitude motions of the intercalated ions, such as, the rotation with conformational changes in the alkyl chain, are restricted due to the small interlayer space even at 400 K.

From comparison of powder patterns between saponite and tetrasilicicfluormica compounds, it is revealed that quite sharp patterns were obtained in mica series while much broad patterns in saponite. This phenomenon points out that interlayer distances in saponite compounds are widely distributed, whereas those in tetrasilicicfluormica ones are relatively homogeneous.

3.2 Elemental Analysis

From elemental analysis, we evaluated the cation exchange ratio from Na^+ to intercalated organocations, i.e., the cationic occupied area on the clay sheet, the free area allocated to it, and the ratio of free area to occupied area and tabulated these data in Table 3.3 and 3.4. The filling ratios, which are given by dividing occupied area by free area, in C81-SP, C81-MC, and C41-MC were more than 75 %, indicating that, in these compounds, organocations fully occupy the area on the clay sheets, that is, they are densely packed in the interlayer spaces. On the other hand, in C41-SP, C82-SP, C82-MC, C42-MC, M3-MC, and M4-MC intercalated ions are filled in the range 40-75 %. Regarding C42-SP, C32-SP, Gu-MC, the filling ratios of less than 40 % were obtained, so it can be mentioned that these ions are in the slightly packed state between the clay sheets as if their state can be considered to be 2D gas.

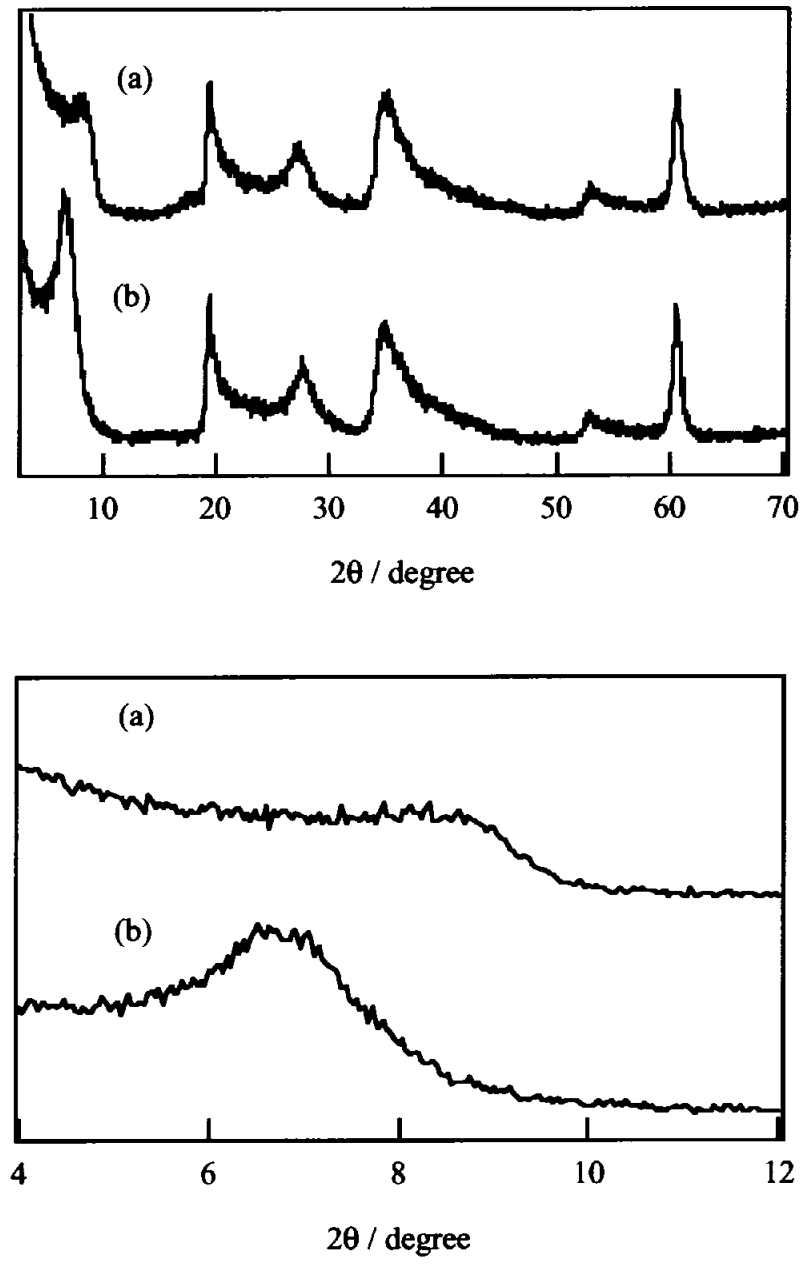

Fig. 3.1. X-Ray powder diffraction patterns observed in Na-saponite (a) at 400 and (b) 300 K. Lower graph is an expansion of a part between 4°-12° in the upper one.

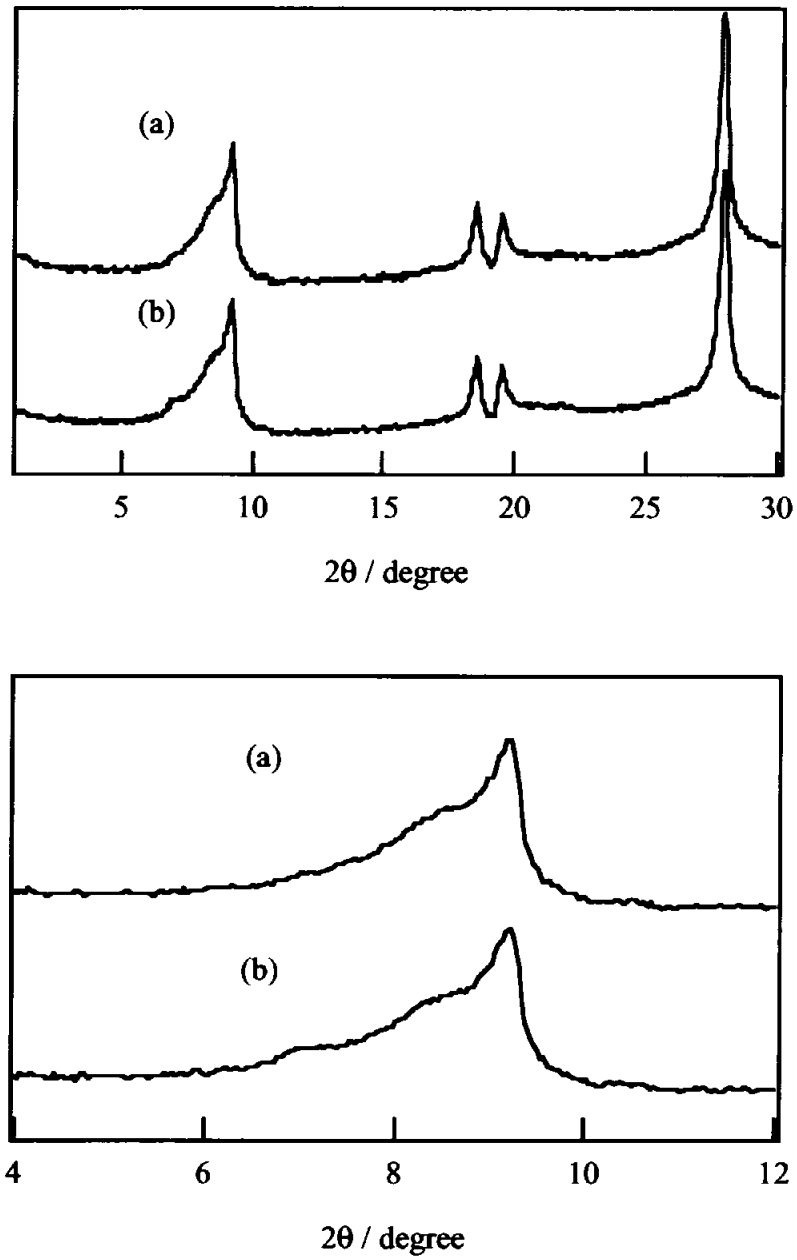

Fig. 3.2. X-Ray powder diffraction patterns observed in Na-tetrasilicicfluormica (a) at 400 and (b) 300 K. Lower graph is an expansion of a part between 4°-12° in the upper one.

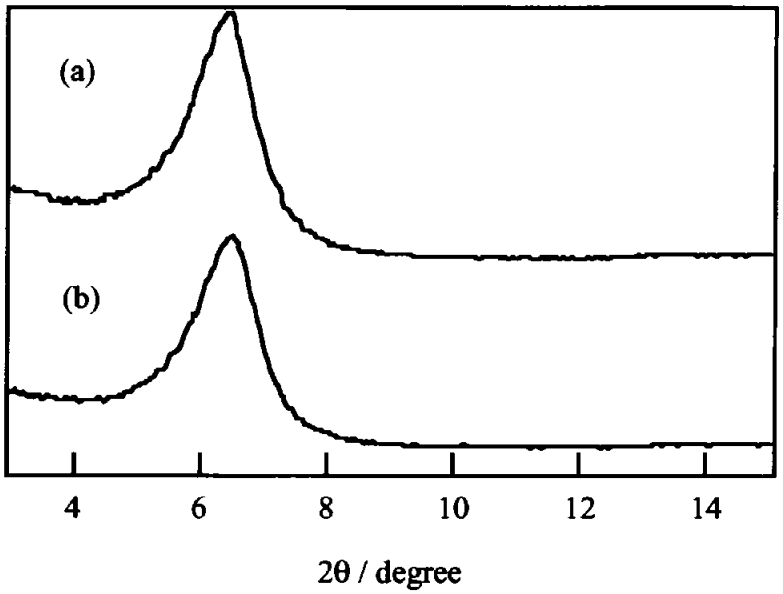

Fig. 3.3. X-Ray powder diffraction patterns observed in $CH_3(CH_2)_7NH_3$-saponite (a) at 400 and (b) 300 K.

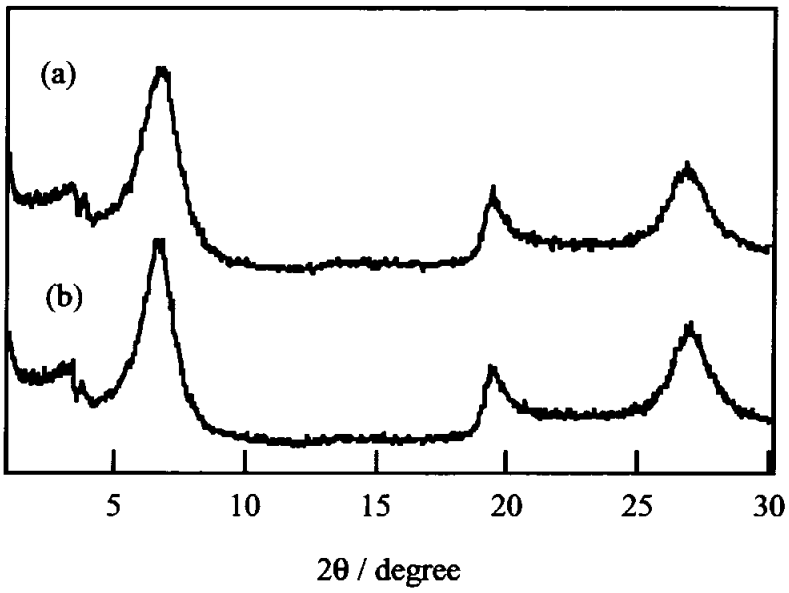

Fig. 3.4. X-Ray powder diffraction patterns observed in $CH_3(CH_2)_3NH_3$-saponite (a) at 400 and (b) 300 K.

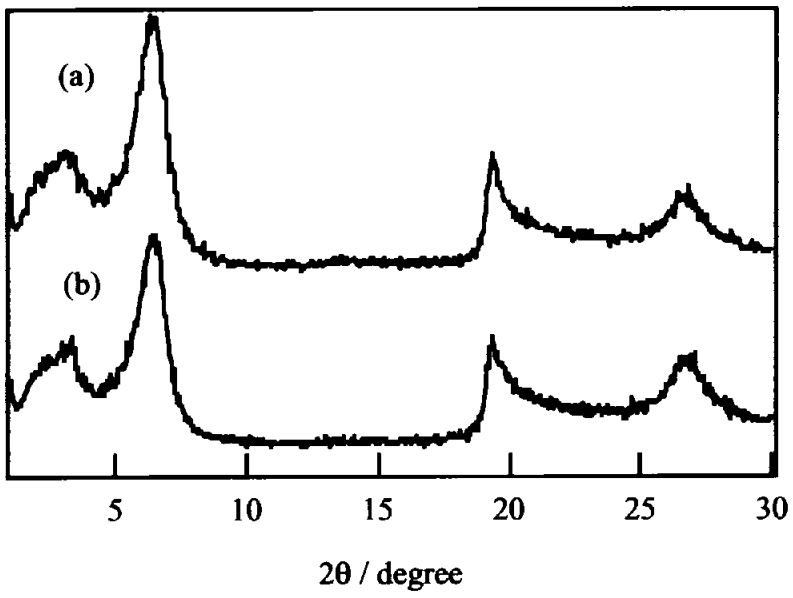

Fig. 3.5. X-Ray powder diffraction patterns observed in $NH_3(CH_2)_8NH_3$-saponite (a) at 400 and (b) 300 K.

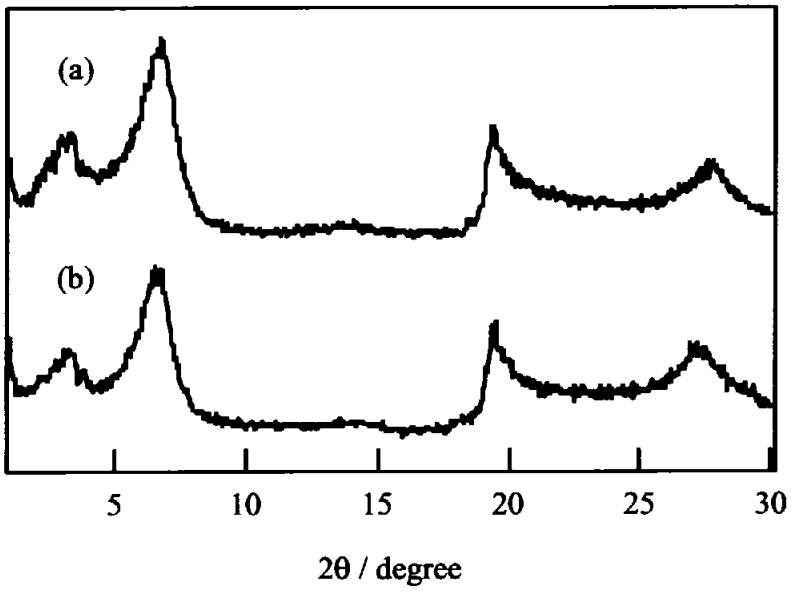

Fig. 3.6. X-Ray powder diffraction patterns observed in $NH_3(CH_2)_4NH_3$-saponite (a) at 400 and (b) 300 K.

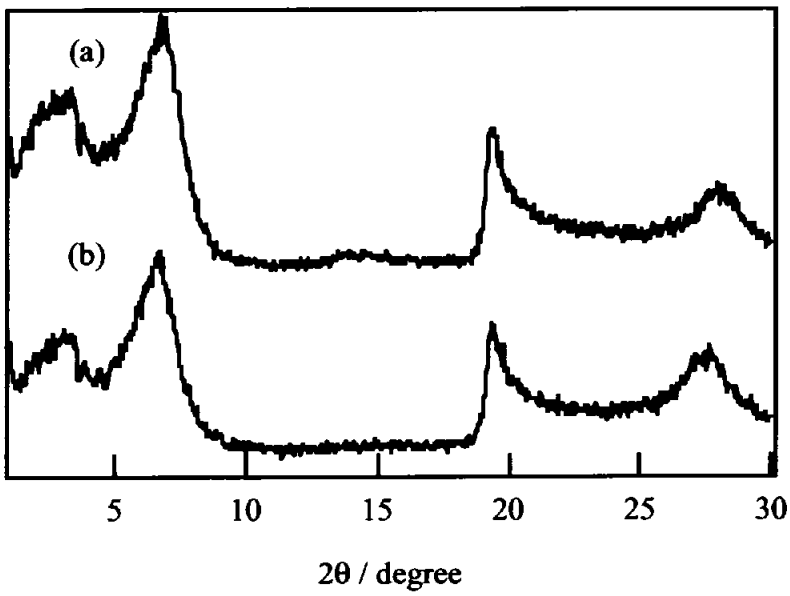

Fig. 3.7. X-Ray powder diffraction patterns observed in $NH_3(CH_2)_3NH_3$-saponite (a) at 400 and (b) 300 K.

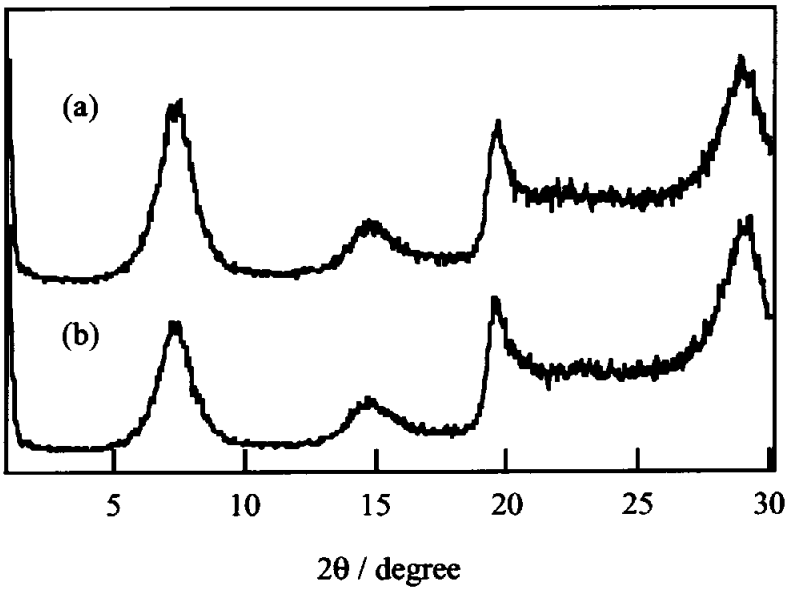

Fig. 3.8. X-Ray powder diffraction patterns observed in $C(NH_2)_3$-saponite (a) at 400 and (b) 300 K.

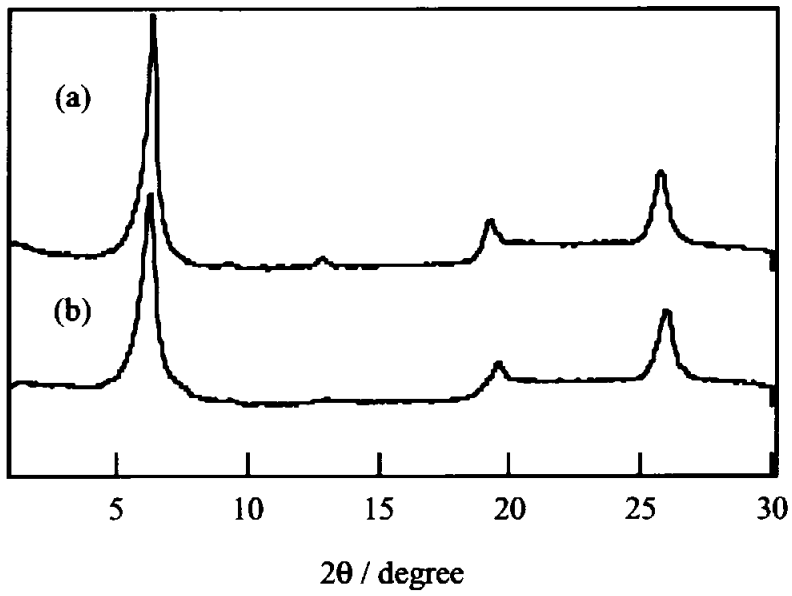

Fig. 3.9. X-Ray powder diffraction patterns observed in $CH_3(CH_2)_7NH_3$-tetrasilicicfluormica (a) at 400 and (b) 300 K.

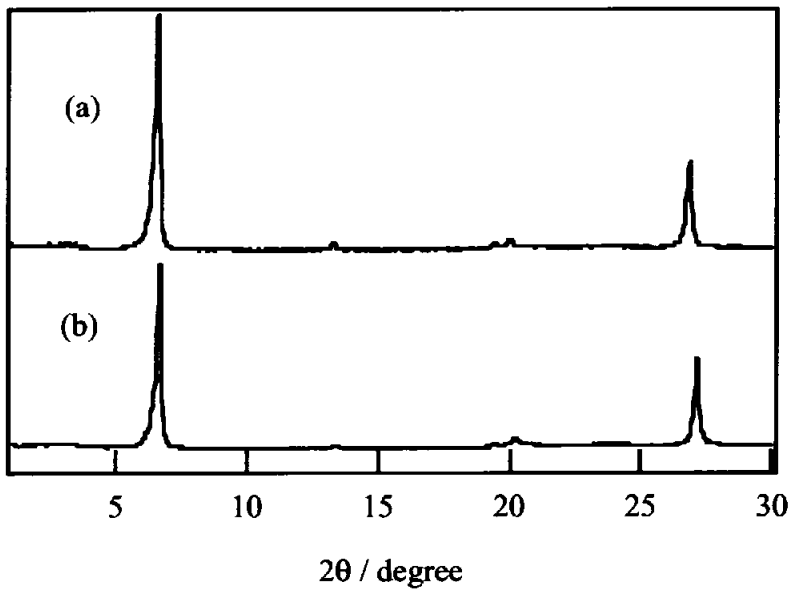

Fig. 3.10. X-Ray powder diffraction patterns observed in $NH_3(CH_2)_8NH_3$-tetrasilicicfluormica (a) at 400 and (b) 300 K.

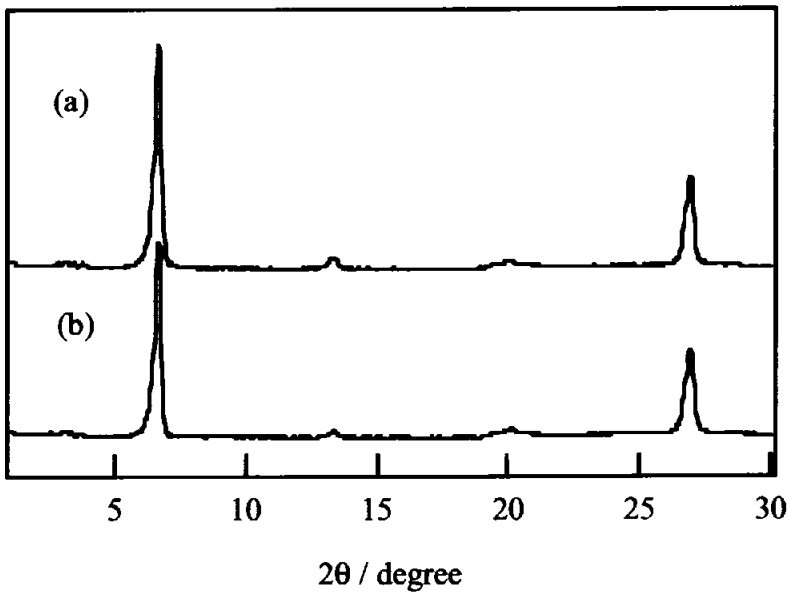

Fig. 3.11. X-Ray powder diffraction patterns observed in $CH_3(CH_2)_3NH_3$-tetrasilicicfluormica (a) at 400 and (b) 300 K.

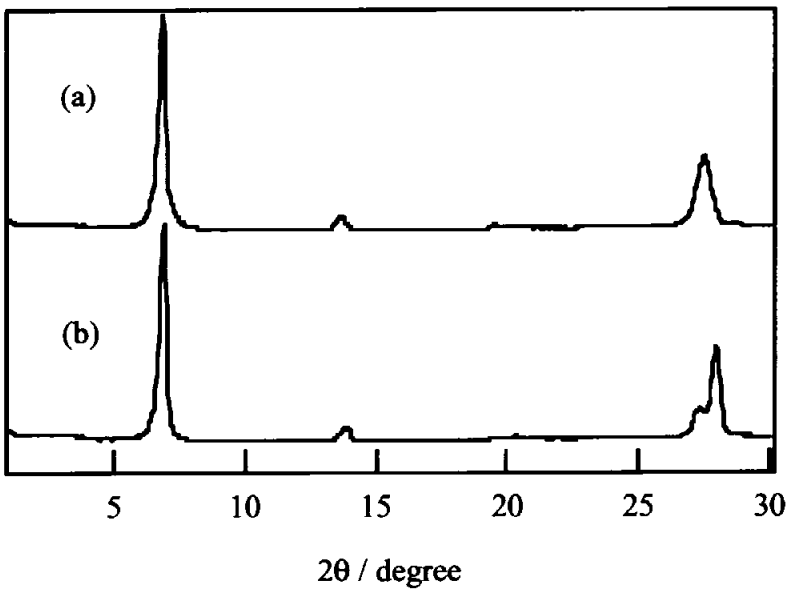

Fig. 3.12. X-Ray powder diffraction patterns observed in $NH_3(CH_2)_4NH_3$-tetrasilicicfluormica (a) at 400 and (b) 300 K.

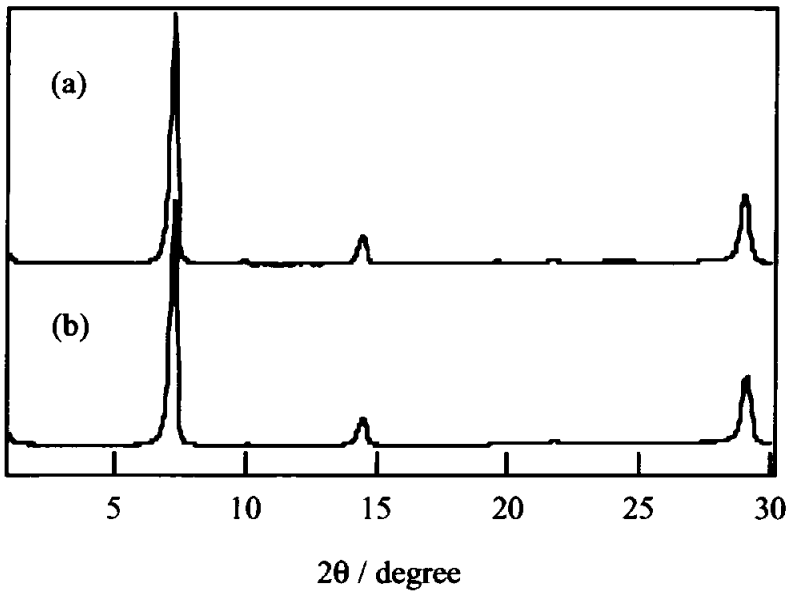

Fig. 3.13. X-Ray powder diffraction patterns observed in $C(NH_2)_3$-tetrasilicicfluormica (a) at 400 and (b) 300 K.

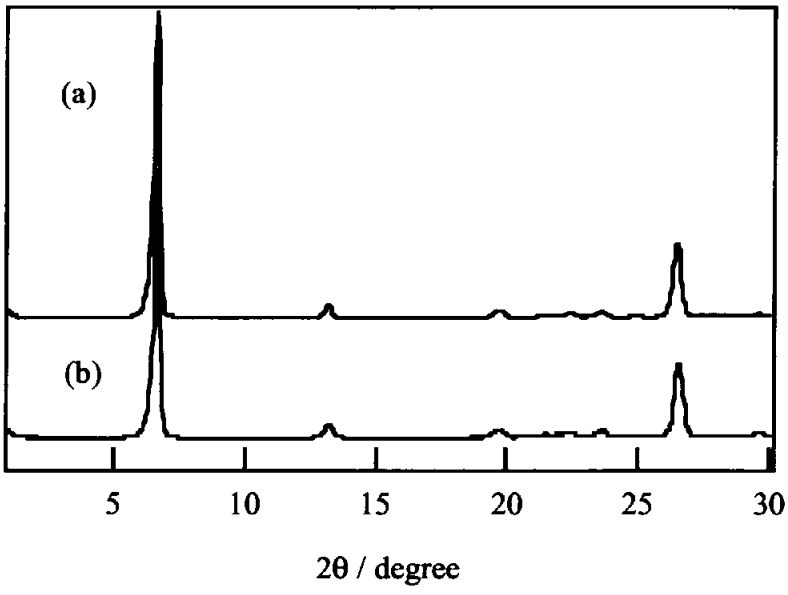

Fig. 3.14. X-Ray powder diffraction patterns observed in $N(CH_3)_4$-tetrasilicicfluormica (a) at 400 and (b) 300 K.

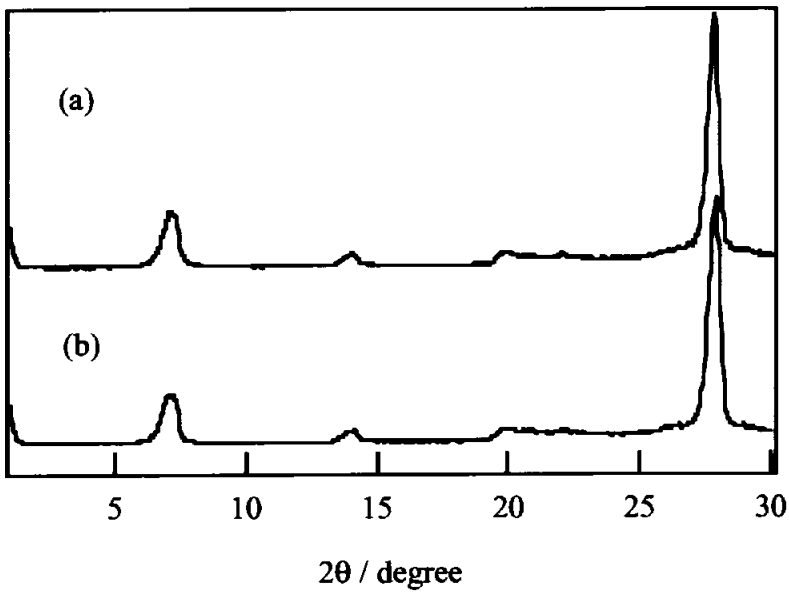

Fig. 3.15. X-Ray powder diffraction patterns observed in $NH(CH_3)_4NH_3$-tetrasilicicfluormica (a) at 400 and (b) 300 K.

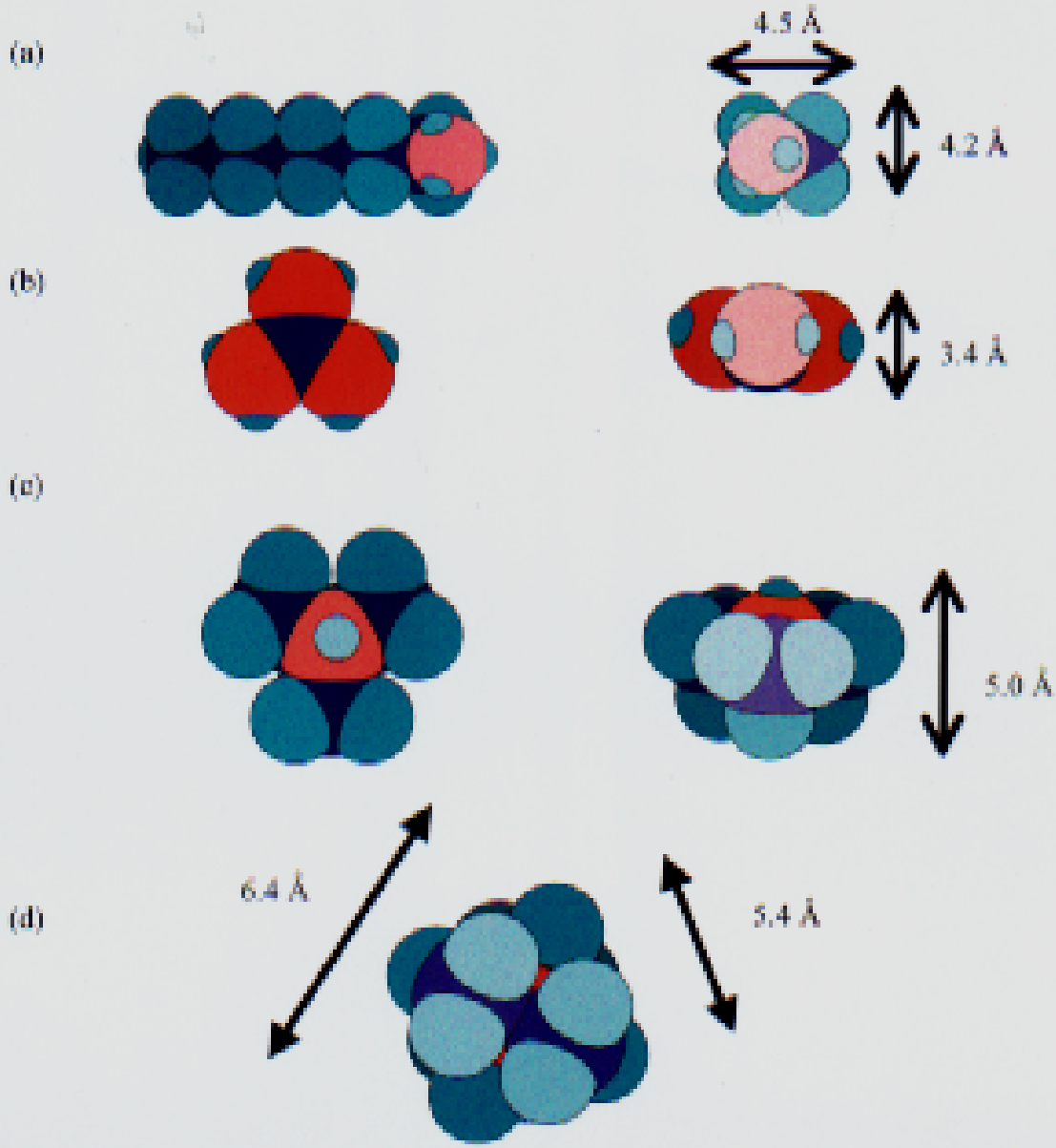

Fig. 3.16. Molecular lenghts in (a)bar-like alkylammonium ions, (b)guanidinium ion, (c) trimethylammonium ion, and (d)tetramethylammonium ion. Length was estimated by using van der Waals radii.

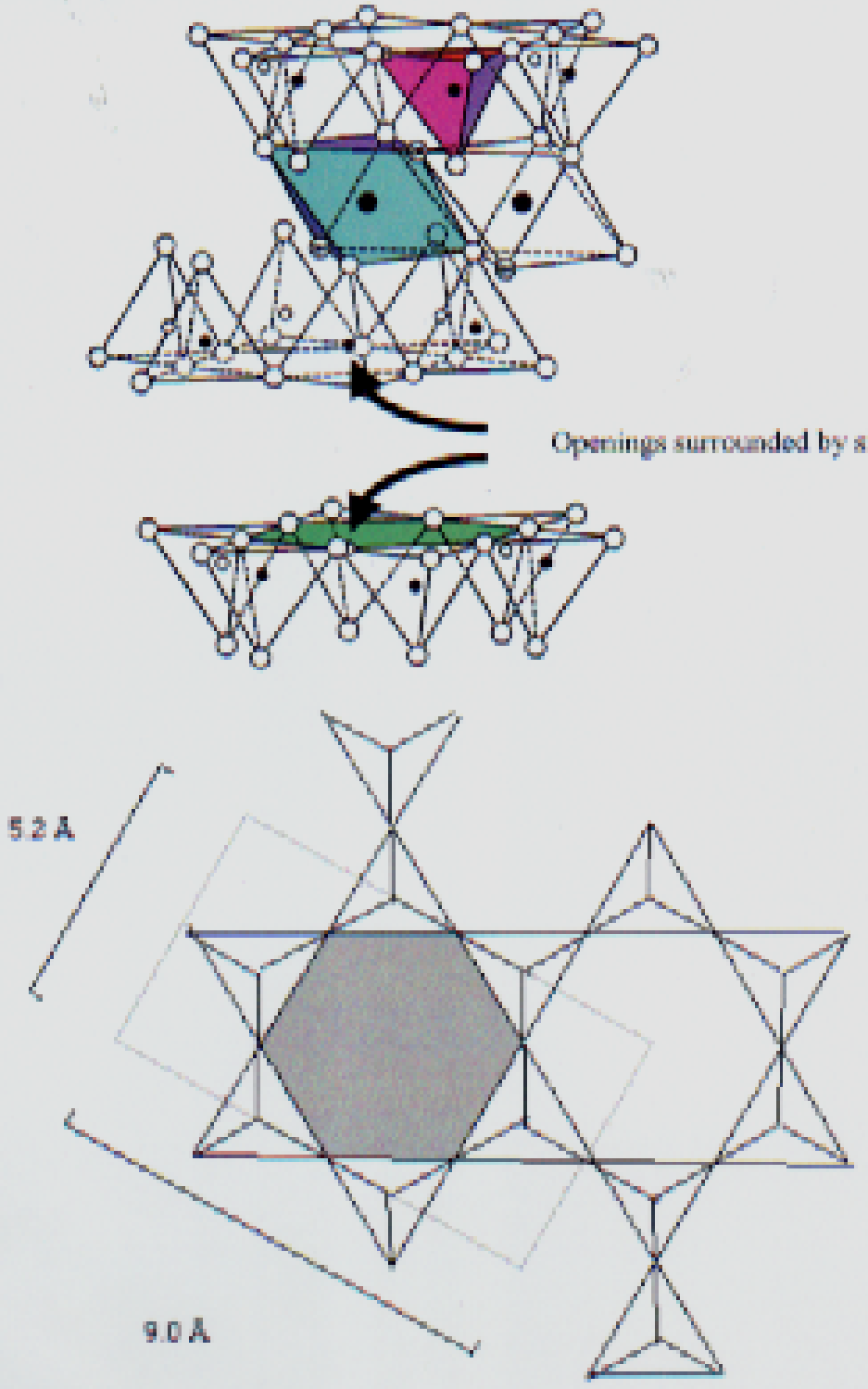

Fig. 3.17. The clay openings made by six surrounding oxygen atoms on the wall.

Table 3.1. *d*(001) spacings in saponite compounds derived from powder X-ray diffraction data obtained at 300 and 400 K. Interlayer distances calculated by subtracting the layer thickness 9.6 Å from respective *d*(001) spacings are shown in parentheses.

sample	interlayer distance / Å	
	300 K	400 K
Na-SP	13.0–2(3.4)	10.2–1(0.60)
C81-SP	13.7–1(4.1)	13.5–1(3.9)
C41-SP	13.1–1(3.5)	13.3–1(3.7)
C82-SP	13.7–1(4.1)	13.5–1(4.1)
C42-SP	13.1–1(3.5)	13.3–1(3.7)
C32-SP	13.2–2(3.6)	13.2–2(3.7)
Gu-SP	12.0–1(2.4)	12.0–1(2.4)

Table 3.2. *d*(001) spacings in tetrasilicicfluormica compounds derived from powder X-ray diffraction data obtained at 300 and 400 K. Interlayer distances calculated by subtracting the layer thickness 9.6 Å from respective *d*(001) spacings are shown in parentheses.

sample	interlayer distance / Å	
	300 K	400 K
Na-MC	9.60–0.5(~0)	9.60–0.5(~0)
C81-MC	14.1–0.5(3.7)	13.8–0.3(3.7)
C82-MC	13.2–0.2(3.6)	13.4–0.2(3.8)
C41-MC	13.3–0.3(3.7)	13.3–0.3(3.7)
C42-MC	12.8–0.4(3.2)	12.9–0.3(3.2)
Gu-MC	12.1–0.2(2.5)	12.1–0.2(2.5)
M4-MC	13.3–0.3(3.7)	13.3–0.3(3.7)
M3-MC	12.4–0.5(2.8)	12.4–0.5(2.8)

Table 3.3. The cation exchange ratio from Na^+ ion to organocations, and the area occupied by a cation on one side of the clay sheet and the free area allocated to it. Filling ratios are given by dividing free area by occupied area.

sample	exchange ratio / %	occupied area / Å^2	free area /Å^2	filling ratio / %
C81-SP	57	60	75	77
C41-SP	57	37	75	50
C82-SP	76	65	110	56
C42-SP	65	43	130	32
C32-SP	67	37	130	29

Table 3.4. The cation exchange ratio from Na^+ ion to organocations, and the area occupied by a cation on one side of the tetrasilicicfluormica sheet and the free area allocated to it. Filling ratios are given by dividing free area by occupied area.

sample	exchange ratio / %	occupied area / Å^2	free area /Å^2	filling ratio / %
C81-MC	57	60	48	130
C82-MC	57	65	100	67
C41-MC	64	37	47	77
C42-MC	67	43	97	43
Gu-MC	58	18	52	35
M4-MC	59	35	51	67
M3-MC	62	35	49	71